Electromechanical field analysis of PN junctions in bent composite piezoelectric semiconductor beams under shear forces

Decai Liu[1, 2], Kai Fang[1, 2], Peng Li[1, 2], Dianzi Liu[3], Zhenghua Qian[1, 2, *]

[1] State Key Laboratory of Mechanics and Control of Mechanical Structures, College of Aerospace Engineering, Nanjing University of Aeronautics and Astronautics, Nanjing 210016, China

[2] Nanjing University of Aeronautics and Astronautics Shenzhen Research Institute, Shenzhen, 518057, China

[3] School of Engineering, University of East Anglia, Norwich, NR4 7TJ, United Kingdom

[*]E-mail: qianzh@nuaa.edu.cn

Tel.: +86-25-84895952, Fax: +86-25-84891422

Abstract: In piezotronics, PN junctions usually possess both piezoelectricity and semiconductor properties. This allows them to be manipulated mechanically by external forces through the coupling between deformation and free carriers. For a conventional non-piezoelectric PN junction, however, the mechanical manipulation seems difficult to achieve. In this paper, we theoretically demonstrate that this problem may be addressed via structural design. A composite beam model consisting of a piezoelectric dielectric layer and two non-piezoelectric PN junction layers is proposed. Then its electromechanical response under three different types of shear loads is examined based on a one-dimensional phenomenological theory. Results show as expected that the electrical behaviors of the junction can be tuned mechanically when the external force is applied on the interface, which provides a new idea for the design of piezotronic devices. Further, the effects of the doping level, thickness ratio, and material combination are also investigated, providing a comprehensive understanding of the proposed composite model.

Keywords: piezoelectric semiconductor, composite structure, PN junction, bending

1. Introduction

In piezoelectric semiconductors (PSs), the free carriers are coupled to the mechanical fields through piezoelectric effect, which allows the semiconductor behavior to be tuned by external force [1]. This unique coupling has been employed to develop a variety of novel electronic devices such as energy harvesters and nanogenerators [2-4], field-effect transistors [5-7], acoustic charge transport devices [8], as well as strain, gas, humidity and chemical sensors [5, 9]. With the development of material science, different types of PS structures, including 1D nanofibers, 2D nanoplates and 3D nanofilms [5, 10, 11] have been successfully synthesized, and the related studies have gradually formed a new research area called piezotronics [12-14]. The fundamental theory of piezotronics consists of the conventional theory of piezoelectricity [15] and the drift-diffusion theory of semiconductors [16], which has been used to solve various problems in PSs, such as vibrations [17, 18], acoustic wave propagations [19], fractures [20-25], as well as field distribution analysis of rods and PN junctions[26-36].

PN junction can be considered as the most basic building block of electronic devices. For a conventional non-piezoelectric PN junction, the current flowing through it is mainly tuned electrically by gate voltage. While for the PS PN junction in piezotronics, it is usually tuned mechanically by force. This is because the potential barrier configuration is coupled to deformation through the piezoelectric effect of the junction itself. Recently, Yang et al. found a particular way to mechanically tune the conventional PN junctions [34]. They proposed a specific layered model, in which the

conventional PN junction layer made of Si is sandwished between two piezoelectric layers. When subjected to bending, the electric field produced by the piezoelectric layers drives free carriers to redistribute and consequently changes the barrier height and width. It should be noted that in their simulations, the Euler-Bernoulli beam theory was used, which means that the shear stress and shear deformation of the beam have been neglected. As is well known, however, when the cantilever beam is under an external shear force and its slenderness ratio is relatively small, the shear deformation will be very significant and the shear stress will dominate near the middle, as shown in Fig. 1. Therefore in this paper, we attempt to propose a composite beam model that can take full advantage of the shear deformation to manipulate conventional PN junctions. Theoretical analyses based on the Timoshenko beam theory will be performed to demonstrate the desired coupling.

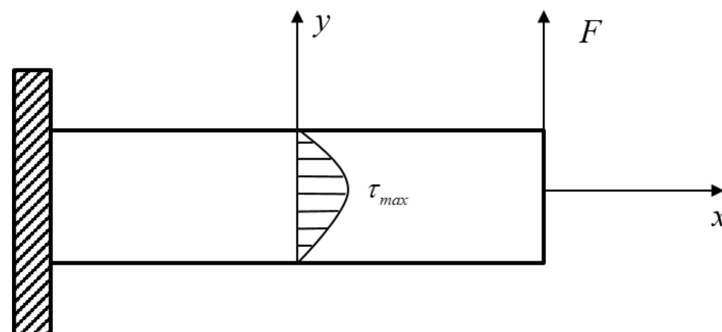

Fig. 1 The shear stress dominates near the middle of the beam under a shear force

The one-dimensional equations for shear bending of the proposed PS composite beam will be introduced in Section 2. The analytical expressions of the coupled electromechanical fields will be derived in Section 3. Then some numerical results and discussions will be given in Section 4. Finally, the conclusions will be summarized in Section 5.

2. One-dimensional equations for the composite beam in shear bending

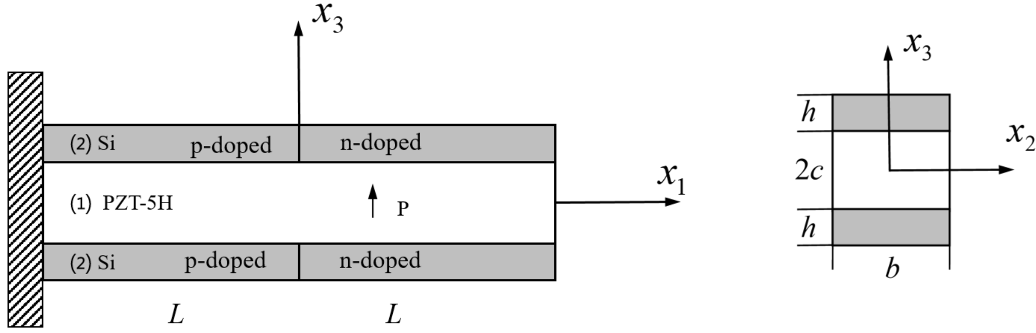

Fig. 2 PN junctions in a composite beam consisting of a non-piezoelectric semiconductor layer and two piezoelectric dielectric layers

Consider the composite fiber shown in Fig. 2. It is composed of a piezoelectric material layer (1) with height $2c$ (e.g., PZT material polarized along the x_3 direction) and two non-piezoelectric semiconductor layers (2) with height h (e.g., Si). The piezoelectric layer is placed in the middle because the shear force is larger there, as shown in Fig. 1. The left halves of the Si layers are holes dominated p type and the right halves are electrons dominated n type. They are both of length L. The left end of the composite beam is fixed. In this situation, the fields can be approximately described as [33]:

$$u_3(x,t) = \omega(x_1,t), \quad u_1(x,t) = x_3\psi(x_1,t), \quad \varphi(x,t) = \varphi(x_1,t), \tag{1}$$

where ω is the bending displacement, Ψ is the thickness shear displacement and φ is the electric potential.

As usual [32-35], the hole concentration p and electron concentration n in the semiconductor layers are respectively denoted by $p = p_0 + \Delta p$ and $n = n_0 + \Delta n$, in which

p_0 and n_0 are their initial concentrations in the unstrained reference state, Δp and Δn their small perturbations. We have:

$$\Delta p \cong \Delta p(x_1, t), \quad \Delta n \cong \Delta n(x_1, t). \tag{2}$$

The one-dimensional field equations are [37]:

$$\begin{aligned} & Q_{,1} = 2b(\rho^{(1)}h + \rho^{(2)}c)\ddot{u}_3, \\ & M_{,1} = Q + \bar{I}\ddot{\psi}, \\ & \hat{D}_{,1} = q(\Delta p - \Delta n)A^{(2)}, \\ & q\frac{\partial}{\partial t}(\Delta p) = -J^{p}_{1,1}, \\ & q\frac{\partial}{\partial t}(\Delta n) = J^{n}_{1,1}, \end{aligned} \tag{3}$$

where Q is the shear force in the cross section, M the bending moment, $\widehat{D}$ the total axial electric displacement in the cross section, q the elementary charge, $A^{(2)}$ the cross-sectional area of the semiconductor layer, $J_1{}^p$ and $J_1{}^n$ the hole and electron current densities in the axial direction. Eq. $(3)_1$ and Eq. $(3)_2$ are Newton's law, Eq. $(3)_3$ is Gauss' law (charge equation of electrostatics), and Eq. $(3)_4$ and $(3)_5$ are the conservation of charge for holes and electrons (continuity equations). The one-dimensional constitutive relations for the proposed model are:

$$\begin{aligned} & Q = \hat{c}\hat{A}(\omega_{,1} + \psi) + \bar{e}_{15}\varphi_{,1}, \\ & M = \bar{D}\psi_{,1}, \\ & \hat{D} = A^{(1)}\bar{e}_{15}(\omega_{,1} + \psi) + \hat{\varepsilon}\hat{A}E_1, \\ & J_1^p = -qp_0\mu_{11}^p\varphi_{,1} - qD_{11}^p(\Delta p)_{,1}, \\ & J_1^n = -qn_0\mu_{11}^n\varphi_{,1} + qD_{11}^n(\Delta n)_{,1}, \end{aligned} \tag{4}$$

in which $\bar{e}_{15}$ is the piezoelectric stress constant of the piezoelectric material. The relevant strain and electric field components are:

$$S_5 = \omega_{,1} + \psi,$$
$$E_1 = -\varphi_{,1}. \tag{5}$$

The material and geometric parameters in Eq. (4) can be expressed as:

$$\bar{D} = \frac{2}{3}bc^3\bar{c}_{11}^{(1)} + \frac{2}{3}b[(c+h)^3 - c^3]\bar{c}_{11}^{(2)},$$
$$A^{(1)} = 2bc,\ \ A^{(2)} = 2bh,\ \ \hat{A} = A^{(1)} + A^{(2)}, \tag{6}$$
$$\hat{c}A = \bar{c}_{55}^{(1)}A^{(1)} + \bar{c}_{55}^{(2)}A^{(2)},\ \ \hat{\varepsilon}\hat{A} = \bar{\varepsilon}_{11}^{(1)}A^{(1)} + \bar{\varepsilon}_{11}^{(2)}A^{(2)}.$$

$$\bar{c}_{11}^{(1)} = 1/s_{11}^{(1)},\ \ \bar{c}_{55}^{(1)} = 1/s_{55}^{(1)},\ \ \bar{e}_{15} = d_{15}/s_{55}^{(1)},$$
$$\bar{\varepsilon}_{11}^{(1)} = \varepsilon_{11}^{(1)} - d_{15}^2/s_{55}^{(1)},\ \ \bar{c}_{11}^{(2)} = 1/s_{11}^{(2)},\ \ \bar{c}_{55}^{(2)} = 1/s_{55}^{(2)}. \tag{7}$$

The Einstein relation is:

$$\frac{\mu_{11}^p}{D_{11}^p} = \frac{\mu_{11}^n}{D_{11}^n} = \frac{q}{k_B T}, \tag{8}$$

μ_{11}^p and μ_{11}^n are the mobility of holes and electrons, D_{11}^p and D_{11}^n are the diffusion coefficients of holes and electrons, k_B is the Boltzmann constant, and T is the Kelvin temperature. The axial electric displacement D can be obtained using the following expression:

$$D = \hat{D}/(A^{(1)} + A^{(2)}). \tag{9}$$

3. Electromechanical fields near the PN junction

Next, the analytical expressions for the field distributions of the PN junction will be derived. From Eq. $(3)_1$ and Eq. $(4)_1$ we have:

$$Q_{,1} = \hat{c}\hat{A}(\omega_{,11} + \psi_{,1}) + \bar{e}_{15}A^{(1)}\varphi_{,11} = 0. \tag{10}$$

From Eq. $(3)_3$ and $(4)_3$, we can derive that:

$$A^{(1)}\bar{e}_{15}(\omega_{,11} + \psi_{,1}) - \hat{\varepsilon}\hat{A}\varphi_{,11} = q(\Delta p - \Delta n)A^{(2)}. \tag{11}$$

Assuming that there's no current flowing through the junction, then Eq. $(4)_4$ and $(4)_5$ give:

$$-qp_0\mu_{11}^p\varphi_{,1} - qD_{11}^p(\Delta p)_{,1} = 0,$$
$$-qn_0\mu_{11}^n\varphi_{,1} + qD_{11}^n(\Delta n)_{,1} = 0. \tag{12}$$

Integrating Eq. (12), we obtain:

$$q\Delta p = -\frac{qp_0\mu_{11}^p}{D_{11}^p}\varphi + C_1,$$
$$-q\Delta n = -\frac{qn_0\mu_{11}^n}{D_{11}^n}\varphi + C_2, \tag{13}$$

Substituting Eq. (13) and (10) into Eq. (11) yields:

$$\varphi_{,11} - \kappa^2\varphi = -\frac{(C_1 + C_2)A^{(2)}}{\varepsilon^*}, \tag{14}$$

where:

$$\varepsilon^* = \frac{(\bar{e}_{15}A^{(1)})^2}{\hat{c}\hat{A}} + \hat{\varepsilon}\hat{A},$$
$$\kappa^2 = \left(\frac{qp_0\mu_{11}^p}{D_{11}^p} + \frac{qn_0\mu_{11}^n}{D_{11}^n}\right)\frac{A^{(2)}}{\varepsilon^*}. \tag{15}$$

The general solution of Eq. (14) is:

$$\varphi = \kappa C_3 \sinh\kappa x_1 + \kappa C_4 \cosh\kappa x_1 + \frac{(C_1 + C_2)A^{(2)}}{\kappa^2\varepsilon^*}, \tag{16}$$

Consider the case that the beam is under an shear force F, then from Eq. $(3)_2$, Eq. $(4)_2$ and $Q = F$, we have:

$$\bar{D}\psi_{,11} = F. \tag{17}$$

The integration of Eq. (17) gives:

$$\psi = \frac{1}{2}\frac{F}{\bar{D}}x_1^2 + C_5 x_1 + C_6, \tag{18}$$

Substituting Eq. (18) into Eq. (10), the integration yields that:

$$\omega = \frac{Fx_1 - \bar{e}_{15}A^{(1)}\varphi + C_7}{\hat{c}\hat{A}} - \int \psi dx_1, \tag{19}$$

In above equations, $C_1 - C_7$ are undetermined constants.

We use a prime to represent the quantities in the left half of the junction, and a double prime to represent those in the right half. For the left half ($x_1 < 0$), we have:

$$\varphi = \kappa' C_3' \sinh \kappa' x_1 + \kappa' C_4' \cosh \kappa' x_1 + \frac{(C_1' + C_2')A^{(2)}}{\kappa'^2 \varepsilon^{*\prime}}, \tag{20}$$

$$\psi = \frac{1}{2}\frac{F}{\overline{D}} x_1^2 + C_5' x_1 + C_6', \tag{21}$$

$$\omega = \frac{Fx_1 - \bar{e}_{15}A^{(1)}\varphi + C_7'}{\hat{c}\hat{A}} - \int \psi dx_1, \tag{22}$$

$$\begin{aligned} q\Delta p &= -\frac{qp_0' \mu_{11}^p}{D_{11}^p}\varphi + C_1', \\ -q\Delta n &= -\frac{qn_0' \mu_{11}^n}{D_{11}^n}\varphi + C_2'. \end{aligned} \tag{23}$$

Similarly, for the right half ($x_1 > 0$), we have:

$$\varphi = \kappa'' C_3'' \sinh \kappa'' x_1 + \kappa'' C_4'' \cosh \kappa'' x_1 + \frac{(C_1'' + C_2'')A^{(2)}}{\kappa''^2 \varepsilon^{*\prime\prime}}, \tag{24}$$

$$\psi = \frac{1}{2}\frac{F}{\overline{D}} x_1^2 + C_5'' x_1 + C_6'', \tag{25}$$

$$\omega = \frac{Fx_1 - \bar{e}_{15}A^{(1)}\varphi + C_7''}{\hat{c}\hat{A}} - \int \psi dx_1, \tag{26}$$

$$\begin{aligned} q\Delta p &= -\frac{qp_0'' \mu_{11}^p}{D_{11}^p}\varphi + C_1'', \\ -q\Delta n &= -\frac{qn_0'' \mu_{11}^n}{D_{11}^n}\varphi + C_2''. \end{aligned} \tag{27}$$

When the external force F is applied on the right end face of the beam, the boundary conditions and the continuity conditions at the interface are:

$$\omega(-L)=0,\ \ \psi(-L)=0,\ \ \hat{D}(-L)=0,\ \ J_1^p(-L)=0,\ \ J_1^n(-L)=0,$$
$$M(L)=0,\ \ Q(L)=F,\ \ \hat{D}(L)=0,\ \ J_1^p(L)=0,\ \ J_1^n(L)=0. \tag{28}$$

$$\omega(0^+)=\omega(0^-),\ \ \psi(0^+)=\psi(0^-),\ \ M(0^+)=M(0^-),\ \ Q(0^+)=Q(0^-),$$
$$\varphi(0^+)=\varphi(0^-),\ \ \hat{D}(0^+)=\hat{D}(0^-),\ \ p(0^+)=p(0^-),\ \ n(0^+)=n(0^-), \tag{29}$$
$$J_1^p(0^+)=J_1^p(0^-),\ \ J_1^n(0^+)=J_1^n(0^-).$$

In order to fix the arbitrary constant in the electric potential, it is necessary to suppose that:

$$\varphi(0)=0. \tag{30}$$

For the electrically neutral beam without end charges and end currents of this paper, Δp and Δn must satisfy the following global charge neutrality condition:

$$\int_{-L}^{L}\Delta p dx_1=0,\ \ \int_{-L}^{L}\Delta n dx_1=0. \tag{31}$$

Only one of Eq. (31) is independent. The other is obtained by integrating Eq. (3) between -L and L and using the boundary and continuity conditions of $\widehat{D}$ in (28) and (29), which means that:

$$\int_{-L}^{L}q(\Delta p-\Delta n)dx_1=0. \tag{32}$$

Substituting Eq. (20)-(27) into (28)-(29) and one of (31) yields a system of equations containing undetermined constants, and they can be solved on a computer using MATLAB.

4. Numerical results and discussion

In this section, the electromechanical fields in the proposed model under three different types of mechanical loads will be investigated. In simulations, we set L = 10 μm, b = 50 nm, h = 10 nm and c = 15 nm. The initial carrier concentrations are assumed to take the following form:

$$
\begin{aligned}
&p_0' = n_0'' = a_0 + \lambda a_0, \\
&n'_0 = p_0'' = 0.7a_0 - \lambda a_0, \qquad (33) \\
&a_0 = 10^{23} m^{-3}.
\end{aligned}
$$

It is obvious that different values of λ correspond to different doping profiles.

4.1. Force on the end face

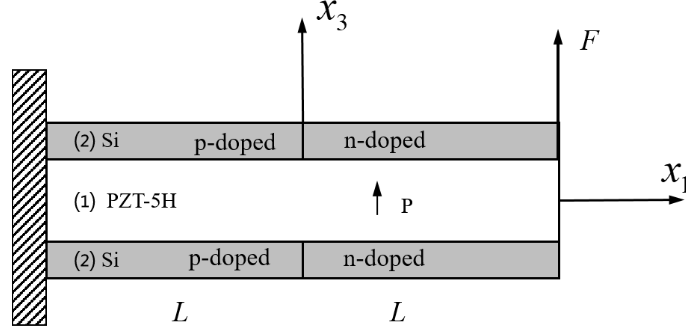

Fig. 3 Composite beam with the shear force F acting on the right end face

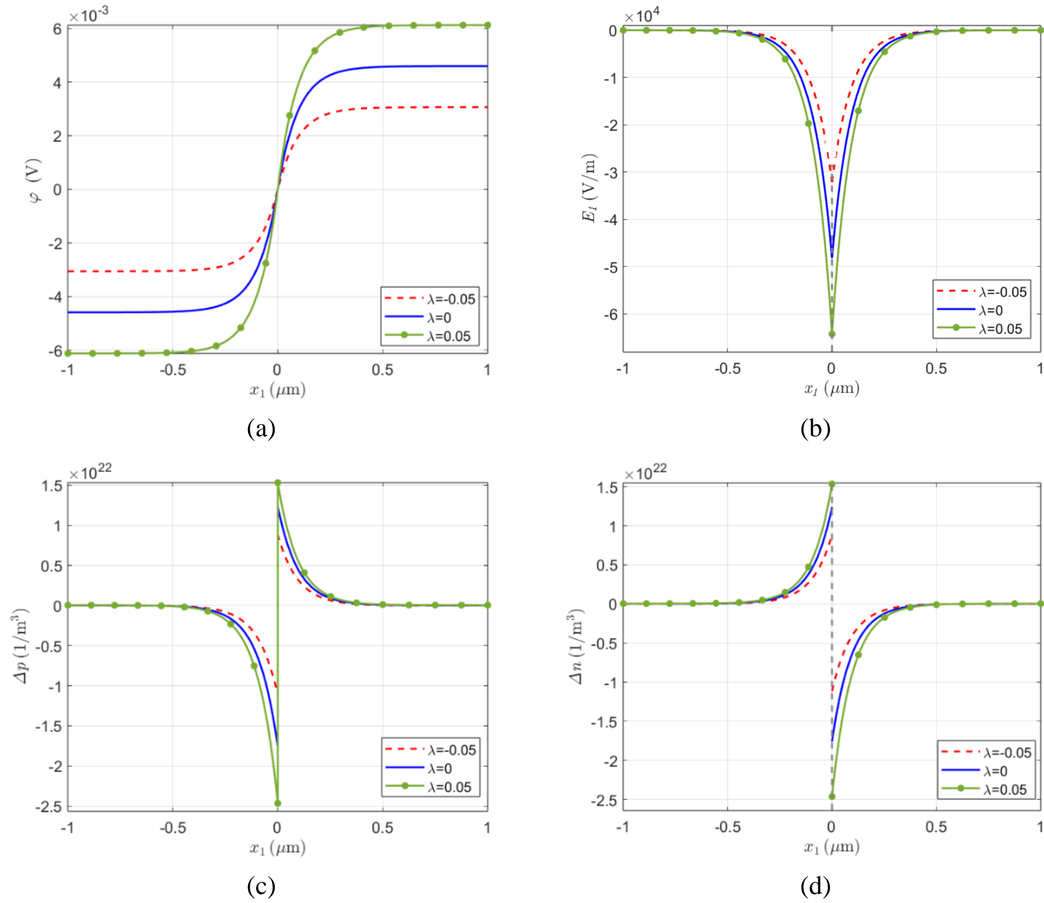

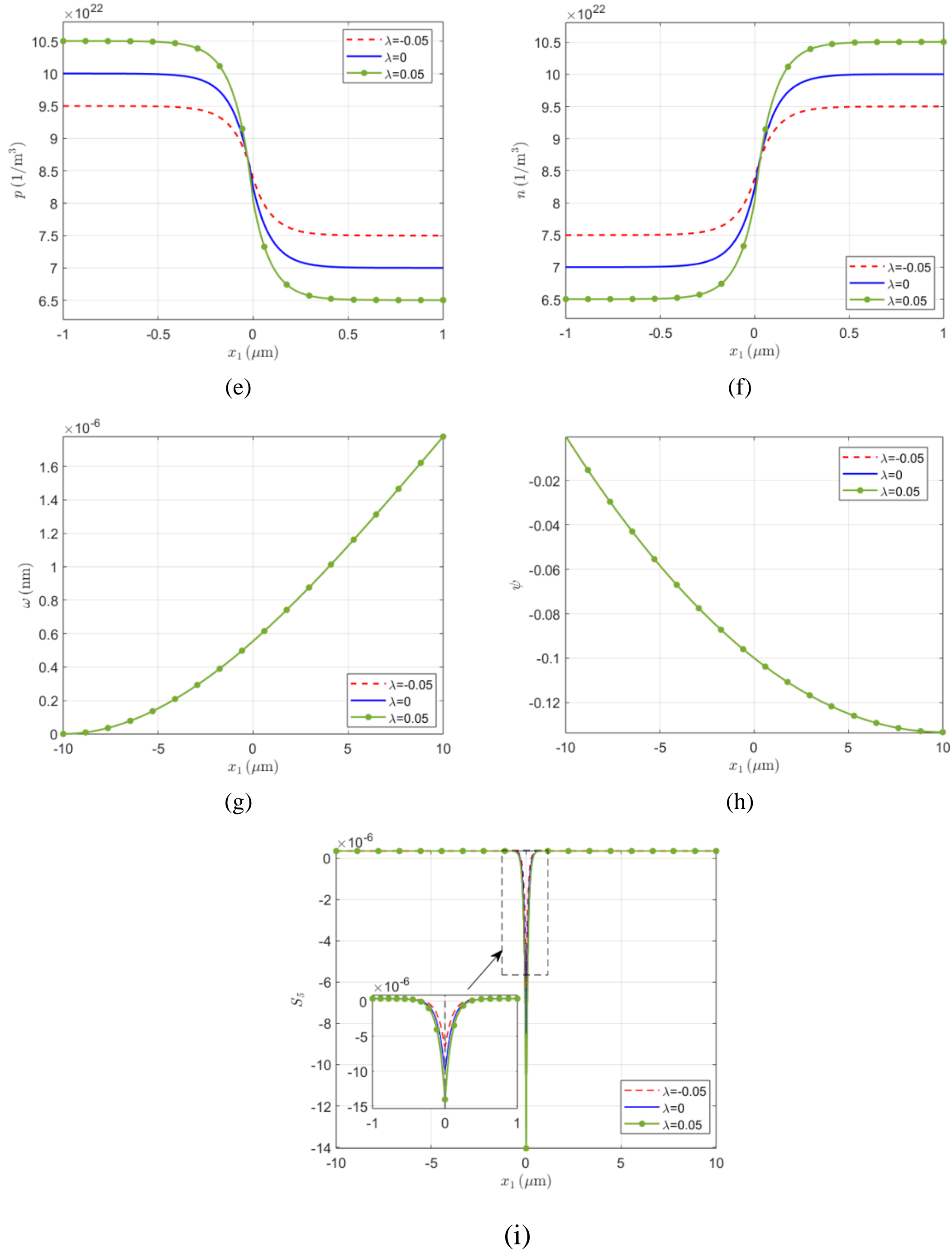

Fig. 4 Electromechanical fields near PN junctions with different doping levels: (a) Electric potential φ; (b) Electric field E; (c) Hole concentration perturbation Δp; (d) Electron concentration perturbation Δn; (e) Hole concentration distribution p; (f) Electron concentration distribution n; (g) Bending displacement ω; (h) Thickness shear displacement Ψ; (i) Shear strain S_5.

Firstly, we investigate the case of the shear force F acting on the right end face of the beam, as shown in Fig. 3. The electromechanical field distributions for different values of λ when F = 40 pN are displayed in Fig. 4. It should be noted that for the electrical fields, only the parts within $|x_1|< 1$ μm are plotted since we are quite interested in their variations near the interface and they have already stabilized at $x_1=\pm 1$ μm. In Fig. 4(a) and (b), the typical electric potential and electric field distributions of PN junctions appear, indicating that the phenomenological coupled theory used in the present paper gives a correct description of the PN junction characteristics. Moreover, a larger λ leads to stronger fields, which is consistent with the conclusion obtained in Ref. [34]. The carrier concentrations and their perturbations are shown in (c)-(f). When λ is large, there are more free carriers in the beam, thus they are more susceptible to perturbation, which is well represented in the figures. The mechanical fields, including the bending displacement ω, the thickness shear displacement Ψ, and the shear strain S_5 are shown in (g)-(i). It can be seen that the variation of doping level hardly affect the distributions of these mechanical fields. This is because they are coupled indirectly through the piezoelectric effect. In addition, to verify the correctness of our linearized model, the comparison of φ in (a) with the results obtained by solving the nonlinear version of Eq. (3) using the finite element method is shown in Appendix. There are minor differences between the curves, but this does not affect the qualitative conclusions in the present paper.

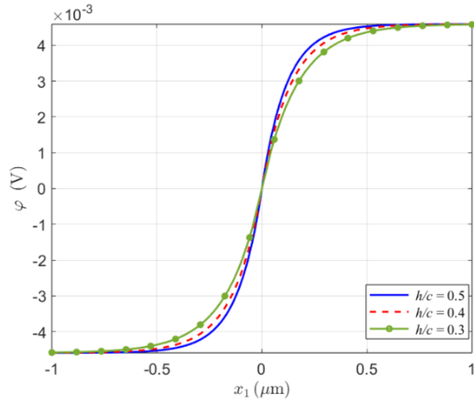

(a)

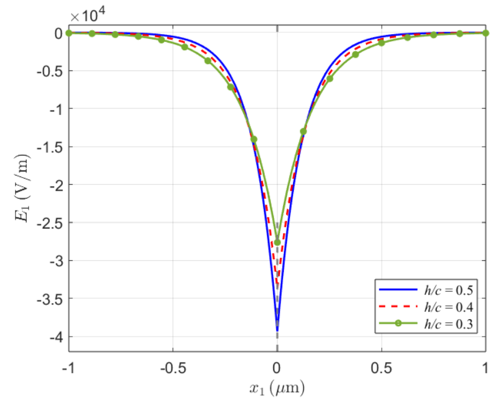

(b)

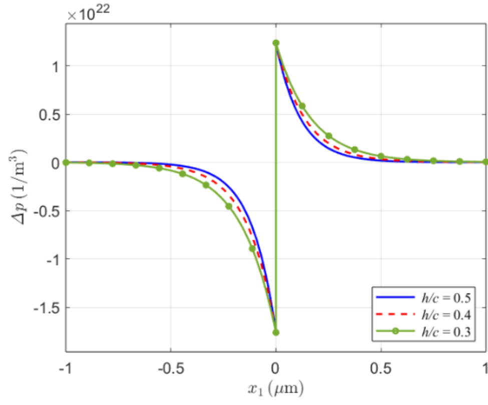

(c)

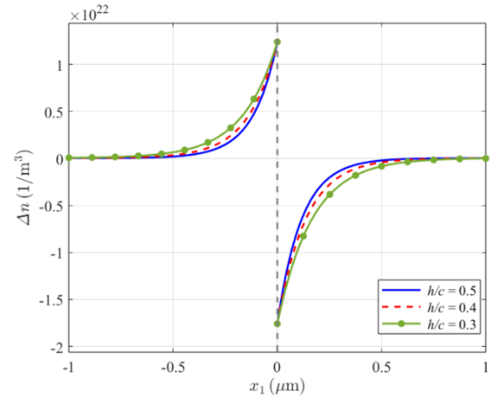

(d)

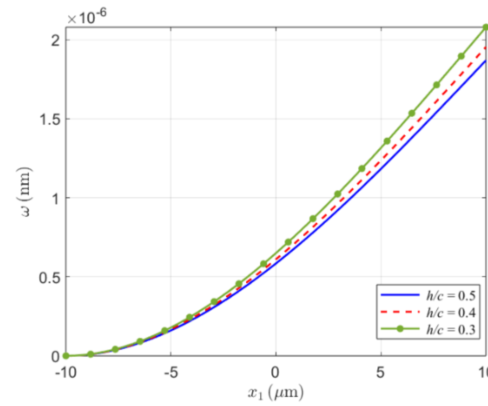

(e)

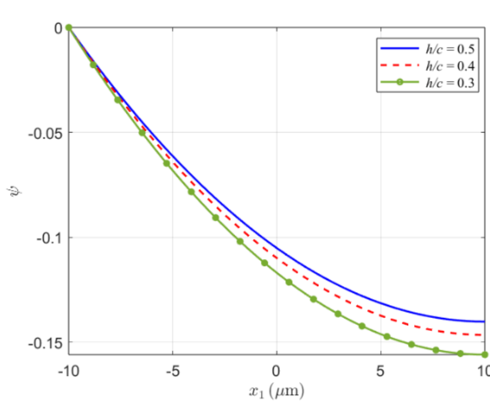

(f)

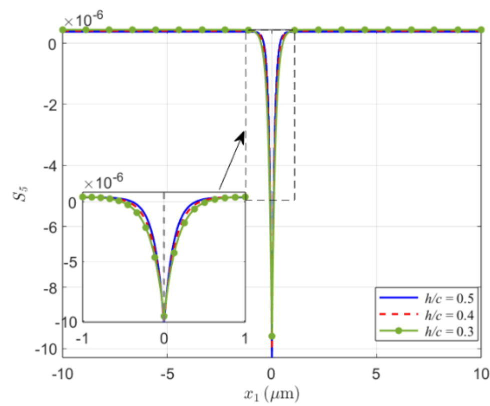

(g)

Fig. 5 Electromechanical fields near PN junctions with different thickness ratios: (a) Electric potential φ; (b) Electric field E; (c) Hole concentration perturbation Δp; (d) Electron concentration perturbation Δn; (e) Bending displacement ω; (f) Thickness shear displacement Ψ; (g) Shear strain S_5.

The effects of the thickness ratio h/c when F = 40 pN are demonstrated in Fig. 5. For a constant $h+c$, as h/c decreases, the semiconductor layers become thinner while the piezoelectric layer becomes thicker. Then the number of mobile charges in the composite fiber must decrease and the piezoelectric coupling will get stronger. Normally, the carrier screen effect should weaken and the electric field should increase at this time. But surprisingly, as shown in (b), E_1 decreases with h/c even if the mechanical fields in (e)-(g) get stronger. This anomaly will be explained later when we study the effects of different values of F.

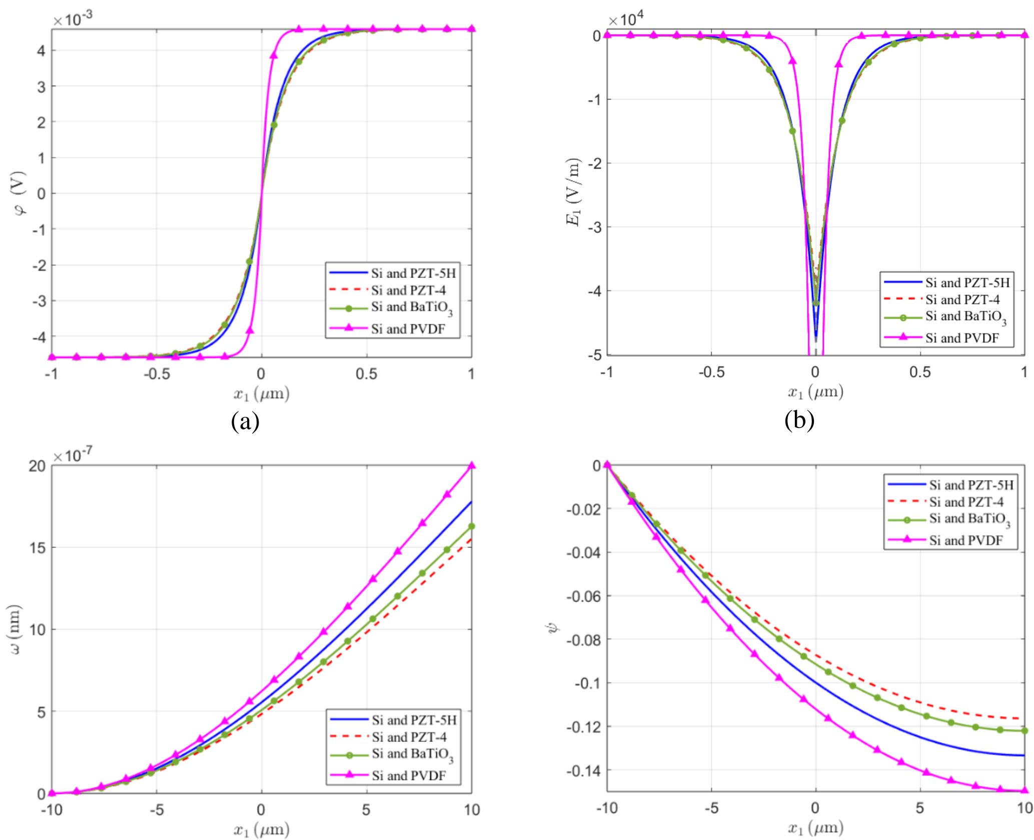

(c) (d)

Fig. 6 Electromechanical fields near PN junctions with different material combinations: (a) Electric potential φ; (b) Electric field E; (c) Bending displacement ω; (d) Thickness shear displacement Ψ.

Fig. 6 shows the influence of different material combinations on the electromechanical field distributions of the PN junction when F is fixed to 40 pN. In simulations, the materials of the piezoelectric layer are chosen to be PZT-5H, PZT-4, $BaTiO_3$ and PVDF, respectively. Their material coefficients are form Ref.[15]. We see that the electrical field distributions for PZT-5H, PZT-4 and $BaTiO_3$ exhibit relatively small differences. This is due to the minor differences in material coefficient between these three materials. In contrast, the curves of PVDF deviate from the rest, which is due to its much smaller piezoelectric coefficient.

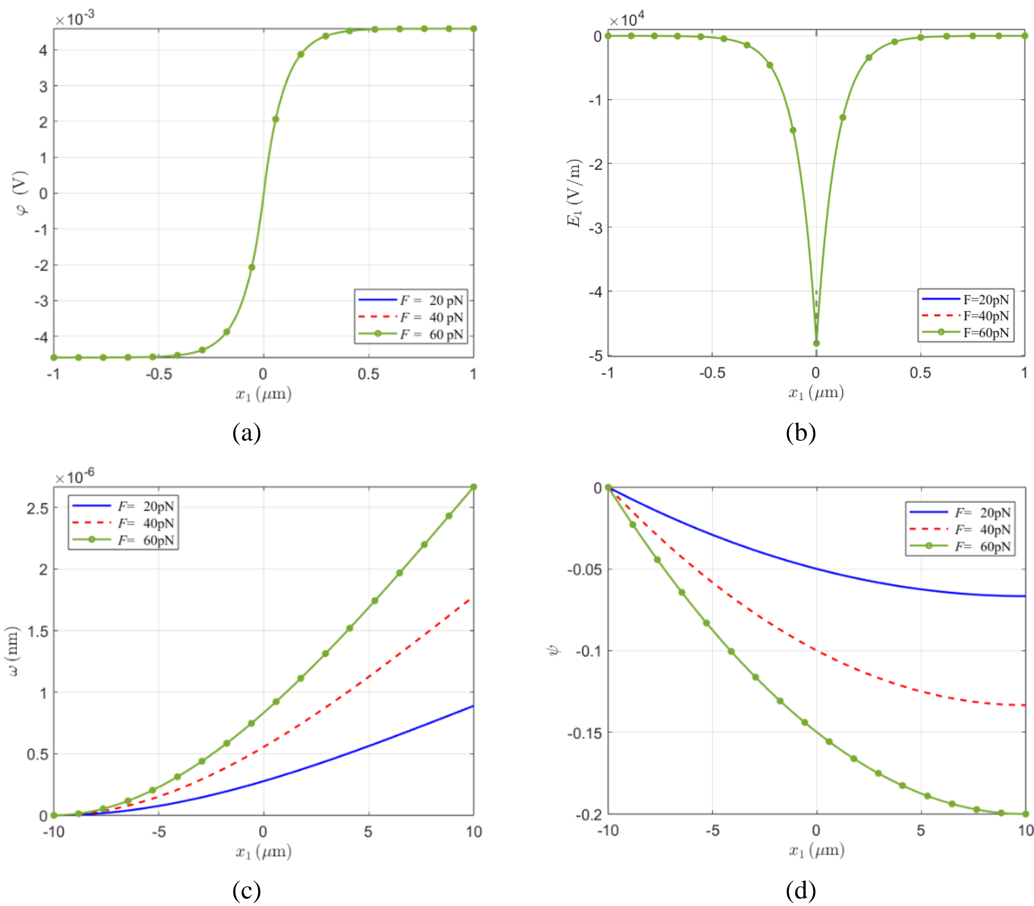

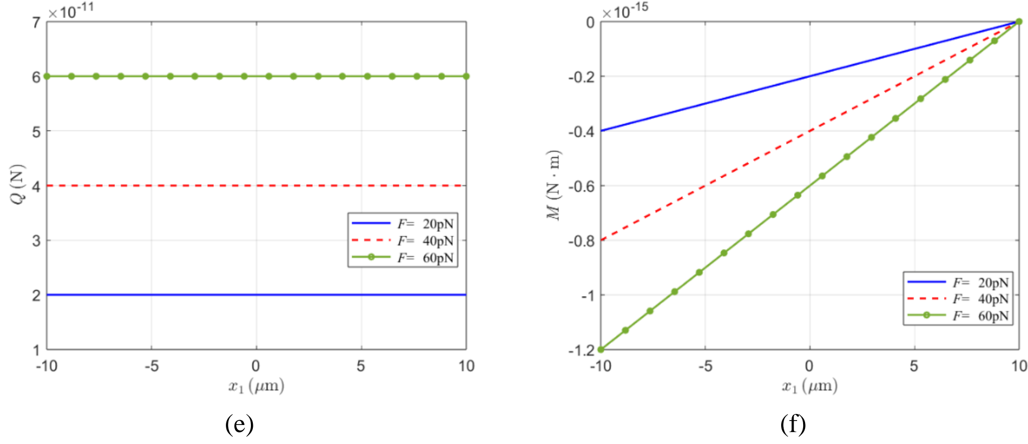

Fig. 7 Electromechanical fields near PN junctions for different values of F: (a) Electric potential φ; (b) Electric field E; (c) Bending displacement ω; (d) Thickness shear displacement Ψ; (e) Shear force Q; (f) Bending moment M.

Fig. 7 shows the field distributions for different values of applied end force F. It can be found that the mechanical fields ω and ψ vary dramatically, while the electrical fields near the interface remains unchanged. This seems to imply that the external shear force cannot be used to manipulate the barrier properties of such a homogeneous PN junction. However, the situation will be different when the action point of the external shear force changes, which will be discussed in the next section. At least, now we see why the electric field decreases with the increase of the mechanical fields in Fig. 5. For such a case where the external shear force acts on the end face, the properties of the PN junction will not be affected by mechanical fields. The decrease of E_1 in Fig. 5(b) is purely caused by the coupling between free carriers and the piezoelectric effect. The distributions of internal shear force Q and bending moment M for different F are plotted in (e) and (f). Q is constant along the beam and M decrease to zero at the right face as expected.

4.2. Force at the interface

In this subsection, the case of the shear force F acting at the PN junction interface is investigated. For the beam in Fig. 8, the boundary conditions become:

$$\begin{aligned} &\omega(-L)=0,\ \ \psi(-L)=0,\ \ \hat{D}(-L)=0,\ \ J_1^p(-L)=0,\ \ J_1^n(-L)=0, \\ &M(L)=0,\ \ Q(0)=F,\ \ \hat{D}(L)=0,\ \ J_1^p(L)=0,\ \ J_1^n(L)=0. \end{aligned} \tag{34}$$

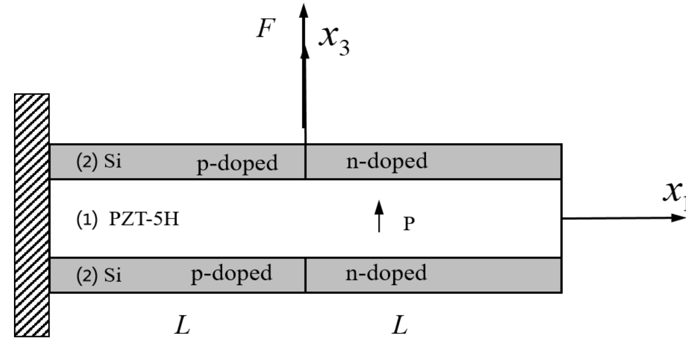

Fig. 8 Composite beam with the shear force F acting at the PN junction interface

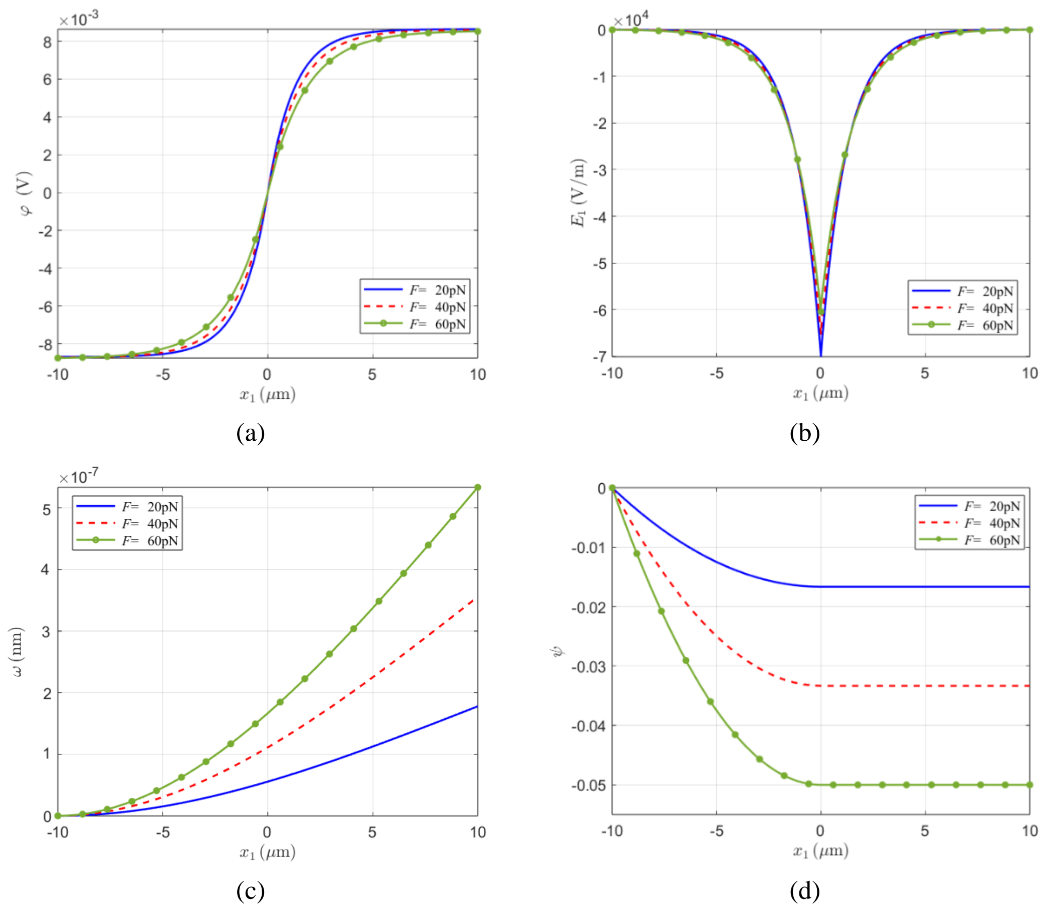

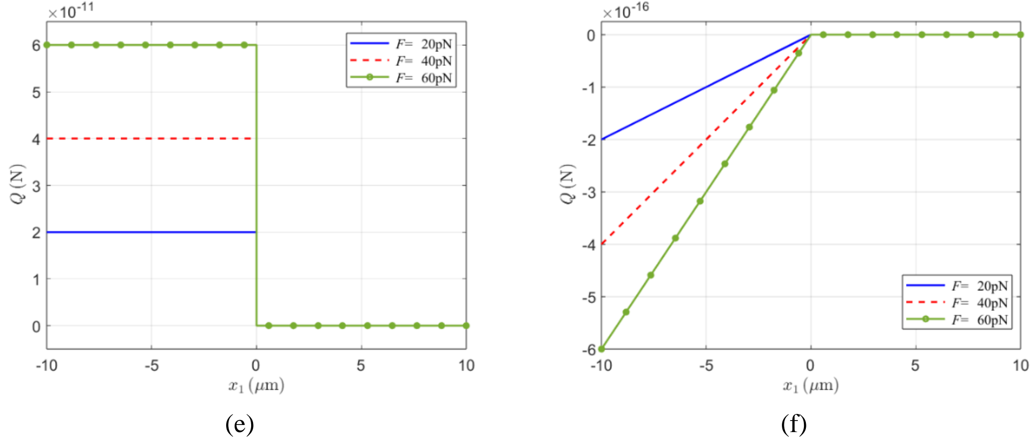

Fig. 9 Electromechanical fields near PN junctions for different values of F. (a) Electric potential φ; (b) Electric field E; (c) Bending displacement ω; (d) Thickness shear displacement Ψ; (e) Shear force Q; (f) Bending moment M.

In Section 4.1, we found that the electrical properties of the junction cannot be tuned by the external end force. However, as shown in Fig. 9 (a) and (b), when the shear force is acting at the interface, the piezoelectric effect is such that the distributions of φ and E will vary with F. This may be developed as a novel tuning approach of homogeneous PS PN junctions. The corresponding mechanical fields are shown in (c) – (f). It shows clearly that the shear force Q and the bending moment M equal to zero at the right half of the beam, which is due to F acting at the interface causing the right part to be stress free.

4.3. Distributed force

When the composite beam is subjected to a distributed force f as shown in Fig. 10, the boundary conditions become:

$$\begin{aligned}&\omega(-L)=0,\quad \psi(-L)=0,\quad \hat{D}(-L)=0,\quad J_1^p(-L)=0,\quad J_1^n(-L)=0,\\&M(L)=0,\quad Q(L)=0,\quad \hat{D}(L)=0,\quad J_1^p(L)=0,\quad J_1^n(L)=0.\end{aligned}\tag{35}$$

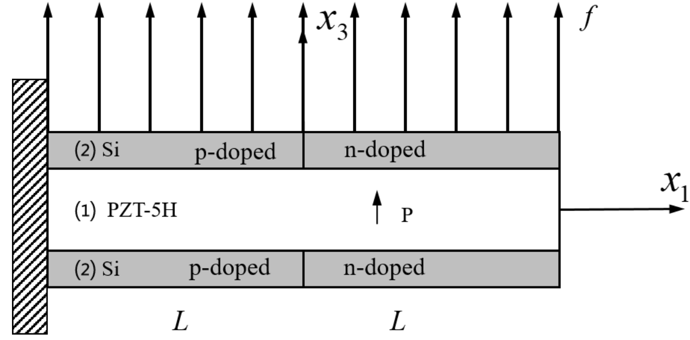

Fig. 10 Composite beam subjected to a distributed force f

(a)

(b)

(c)

(d)

(e)

(f)

Fig. 11 Electromechanical fields near the PN junction for different values of distributed force f: (a) Electric potential φ; (b) Electric field E; (c) Bending displacement ω; (d) Thickness shear displacement Ψ; (e) Shear force Q; (f) Bending moment M.

The electromechanical field distributions are displayed in Fig. 11. Similar to Fig. 7, for different values of f, the electrical fields in (a) and (b) remain almost unchanged. That's to say, the distributed force is similarly not applicable to the manipulation of homogeneous junctions. The values of Q are no longer constants and the curves of M are no longer linear, which is different to Fig. 7 and is not surprising.

5. Conclusions

In this paper, the electromechanical field distributions of the PN junction in a composite beam consisting of a piezoelectric dielectric layer and two non-piezoelectric semiconductor layers are investigated. It is suitable for the bending of PN junctions under shear deformation or shear force. Based on the macroscopic piezoelectric semiconductor theory, the effects of the doping level, thickness ratio, and material combination are systematically studied. Analytical results show that homogeneous junctions are difficult to be tuned by external shear force unless the action point locates near the interface. This may provide a new approach to the mechanical manipulation of conventional PN junctions when shear force dominates.

In addition, the indirect piezoelectric effect of composite structures composed of piezoelectric media and non piezoelectric semiconductors provides a novel approach

for the design of piezoelectric devices. In the future, more in-depth theoretical and experimental research should be conducted on this issue.

Acknowledgments

This work was supported by the National Natural Science Foundation of China (12061131013, 11972276, 12172171, and 12211530064), the State Key Laboratory of Mechanics and Control of Mechanical Structures at NUAA (No. MCMS-I-0522G01), the Fundamental Research Funds for the Central Universities (NS2022011 and NE2020002), National Natural Science Foundation of Jiangsu Province (BK20211176), Local Science and Technology Development Fund Projects Guided by the Central Government (2021Szvup061), Jiangsu High-Level Innovative and Entrepreneurial Talents Introduction Plan (Shuangchuang Doctor Program, JSSCBS20210166), and a project funded by the Priority Academic Program Development of Jiangsu Higher Education Institutions (PAPD).

Appendix

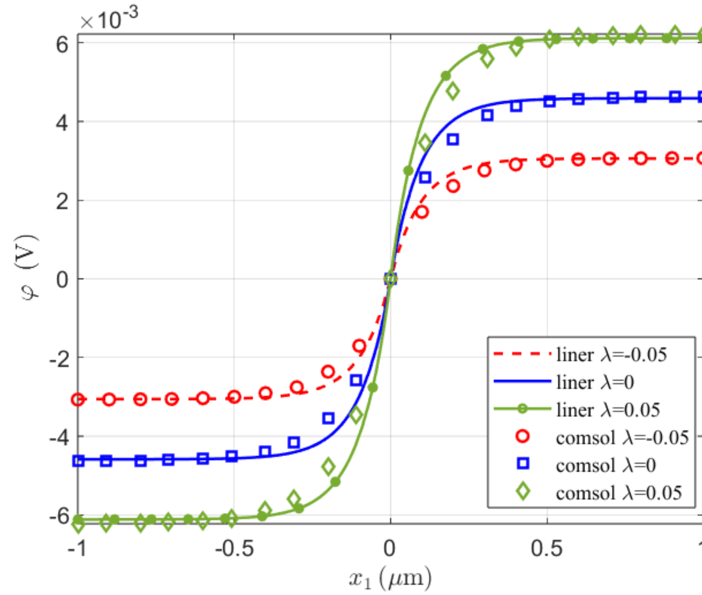

Fig. A Comparison of the linear analytical and nonlinear numerical results

In Fig. A, it can be seen that the difference between the linearization theory derived in this paper and the nonlinear solution of COMSOL is relatively small, which can verify the correctness of the theory in this paper.

References

[1] HICKERNELL, F. S. The piezoelectric semiconductor and acoustoelectronic device development in the sixties. *IEEE Trans Ultrason Ferroelectr Freq Control,* **52**(5), 737-745 (2005).

[2] GAO, P. X., SONG, J. H., LIU, J., WANG, Z. L. Nanowire piezoelectric nanogenerators on plastic substrates as flexible power sources for nanodevices. *Advanced Materials,* **19**(1), 67-72 (2007).

[3] CHOI, M. Y., CHOI, D., JIN, M. J., KIM, I., KIM, S. H., CHOI, J. Y., LEE, S. Y., KIM, J. M., KIM, S. W. Mechanically Powered Transparent Flexible Charge-Generating Nanodevices with Piezoelectric ZnO Nanorods. *Advanced Materials,* **21**(21), 2185-2189 (2009).

[4] ROMANO, G., MANTINI, G., DI CARLO, A., D'AMICO, A., FALCONI, C., WANG, Z. L. Piezoelectric potential in vertically aligned nanowires for high output nanogenerators. *Nanotechnology,* **22**(46), 465401 (2011).

[5] WANG, Z. L. Nanobelts, nanowires, and nanodiskettes of semiconducting oxides—from materials to nanodevices. *Advanced Materials,* **15**(5), 432-436 (2003).

[6] WANG, X., ZHOU, J., SONG, J., LIU, J., XU, N., WANG, Z. L. Piezoelectric field effect transistor and nanoforce sensor based on a single ZnO nanowire. *Nano Lett,* **6**(12), 2768-2772 (2006).

[7] WANG, Z. L. Piezopotential gated nanowire devices: Piezotronics and piezo-phototronics. *Nano Today,* **5**(6), 540-552 (2010).

[8] BüYüKKöSE, S., HERNANDEZ-MINGUEZ, A., VRATZOV, B., SOMASCHINI, C., GEELHAAR, L., RIECHERT, H., VAN DER WIEL, W., SANTOS, P. High-frequency acoustic charge transport in GaAs nanowires. *Nanotechnology,* **25**(13), 135204 (2014).

[9] YU, J., IPPOLITO, S. J., WLODARSKI, W., STRANO, M., KALANTAR-ZADEH, K. Nanorod based Schottky contact gas sensors in reversed bias condition. *Nanotechnology,* **21**(26), 265502 (2010).

[10] WEN, X. N., WU, W. Z., DING, Y., WANG, Z. L. Piezotronic Effect in Flexible Thin-film Based Devices. *Advanced Materials,* **25**(24), 3371-3379 (2013).

[11] LEE, K. Y., KUMAR, B., SEO, J. S., KIM, K. H., SOHN, J. I., CHA, S. N., CHOI, D., WANG, Z. L., KIM, S. W. p-Type polymer-hybridized high-performance piezoelectric nanogenerators. *Nano Lett,* **12**(4), 1959-1964 (2012).

[12] LIU, Y., ZHANG, Y., YANG, Q., NIU, S. M., WANG, Z. L. Fundamental theories of piezotronics and piezo-phototronics. *Nano Energy,* **14**, 257-275 (2015).

[13] WANG, Z. L., WU, W. Z. Piezotronics and piezo-phototronics: fundamentals and applications. *National Science Review,* **1**(1), 62-90 (2014).

[14] WANG, Z. L. *Piezotronics and Piezo-phototronics*: Springer; (2012).

[15] AULD, B. A. *Acoustic fields and waves in solids*: Рипол Классик; (1973).

[16] PIERRET, R. F., NEUDECK, G. W. *Advanced semiconductor fundamentals*: Addison-Wesley Reading, MA; (1987).

[17] WAUER, J., SUHERMAN, S. Thickness vibrations of a piezo-semiconducting plate layer. *International Journal of Engineering Science,* **35**(15), 1387-1404 (1997).

[18] LI, P., JIN, F., YANG, J. S. Effects of semiconduction on electromechanical energy conversion in piezoelectrics. *Smart Materials and Structures,* **24**(2), 025021 (2015).

[19] GU, C. L., JIN, F. Shear-horizontal surface waves in a half-space of piezoelectric semiconductors. *Philosophical Magazine Letters,* **95**(2), 92-100 (2015).

[20] HU, Y. T., ZENG, Y., YANG, J. S. A mode III crack in a piezoelectric semiconductor of crystals with 6 mm symmetry. *International Journal of Solids and Structures,* **44**(11-12), 3928-3938 (2007).

[21] SLADEK, J., SLADEK, V., PAN, E., YOUNG, D. L. Dynamic Anti-plane Crack Analysis in Functional Graded Piezoelectric Semiconductor Crystals. *Cmes-Computer Modeling in Engineering & Sciences,* **99**(4), 273-296 (2014).

[22] SLADEK, J., SLADEK, V., PAN, E., WUNSCHE, M. Fracture analysis in

piezoelectric semiconductors under a thermal load. *Engineering Fracture Mechanics,* **126**, 27-39 (2014).

[23] ZHAO, M. H., PAN, Y. B., FAN, C. Y., XU, G. T. Extended displacement discontinuity method for analysis of cracks in 2D piezoelectric semiconductors. *International Journal of Solids and Structures,* **94-95**, 50-59 (2016).

[24] FAN, C. Y., YAN, Y., XU, G. T., ZHAO, M. H. Piezoelectric-conductor iterative method for analysis of cracks in piezoelectric semiconductors via the finite element method. *Engineering Fracture Mechanics,* **165**, 183-196 (2016).

[25] ZHAO, M. H., LI, Y., YAN, Y., FAN, C. Y. Singularity analysis of planar cracks in three-dimensional piezoelectric semiconductors via extended displacement discontinuity boundary integral equation method. *Engineering Analysis with Boundary Elements,* **67**, 115-125 (2016).

[26] ZHANG, C. L., WANG, X. Y., CHEN, W. Q., YANG, J. S. Carrier distribution and electromechanical fields in a free piezoelectric semiconductor rod. *Journal of Zhejiang University-Science A,* **17**(1), 37-44 (2016).

[27] ZHANG, C. L., WANG, X. Y., CHEN, W. Q., YANG, J. S. Propagation of extensional waves in a piezoelectric semiconductor rod. *Aip Advances,* **6**(4), 045301 (2016).

[28] ZHANG, C. L., WANG, X. Y., CHEN, W. Q., YANG, J. S. An analysis of the extension of a ZnO piezoelectric semiconductor nanofiber under an axial force. *Smart Materials and Structures,* **26**(2), 025030 (2017).

[29] CHENG, R. R., ZHANG, C. L., CHEN, W. Q., YANG, J. S. Piezotronic effects in

the extension of a composite fiber of piezoelectric dielectrics and nonpiezoelectric semiconductors. *Journal of Applied Physics,* **124**(6), 064506 (2018).

[30] ZHANG, C., LUO, Y., CHENG, R., WANG, X. Electromechanical fields in piezoelectric semiconductor nanofibers under an axial force. *MRS Advances,* **2**(56), 3421-3426 (2017).

[31] GAO, Y., WANG, Z. L. Electrostatic potential in a bent piezoelectric nanowire. The fundamental theory of nanogenerator and nanopiezotronics. *Nano Lett,* **7**(8), 2499-2505 (2007).

[32] LUO, Y. X., ZHANG, C. L., CHEN, W. Q., YANG, J. S. Piezopotential in a bended composite fiber made of a semiconductive core and of two piezoelectric layers with opposite polarities. *Nano Energy,* **54**, 341-348 (2018).

[33] FANG, K., QIAN, Z. H., YANG, J. S. Piezopotential in a composite cantilever of piezoelectric dielectrics and nonpiezoelectric semiconductors produced by shear force through e(15). *Materials Research Express,* **6**(11), 115917 (2019).

[34] YANG, G. Y., YANG, L., DU, J. K., WANG, J., YANG, J. S. PN junctions with coupling to bending deformation in composite piezoelectric semiconductor fibers. *International Journal of Mechanical Sciences,* **173**, 105421 (2020).

[35] LUO, Y. X., ZHANG, C. L., CHEN, W. Q., YANG, J. S. An analysis of PN junctions in piezoelectric semiconductors. *Journal of Applied Physics,* **122**(20), 204502 (2017).

[36] YANG, G. Y., DU, J. K., WANG, J., YANG, J. S. Electromechanical Fields in a Nonuniform Piezoelectric Semiconductor Rod. *Journal of Mechanics of Materials*

and Structures, **13**(1), 103-120 (2018).

[37] FANG, K., QIAN, Z., YANG, J. Piezopotential in a composite cantilever of piezoelectric dielectrics and nonpiezoelectric semiconductors produced by shear force through e15. *Materials Research Express,* **6**(11) (2019).